B. Barone[1,2], R. M. Letelier[3], K. H. Rubin[4], and D. M. Karl[1,2]

[1]Daniel K. Inouye Center for Microbial Oceanography: Research and Education, University of Hawai i at Mānoa, Honolulu, HI, USA

[2]Department of Oceanography, University of Hawai i at Mānoa, Honolulu, HI, USA

[3]College of Earth, Ocean, and Atmospheric Sciences, Oregon State University, Corvallis, OR, USA

[4]Department of Earth Sciences, University of Hawai i at Mānoa, Honolulu, HI, USA

Corresponding author: Benedetto Barone (benedetto.barone@gmail.com)

Key Points:

- An extensive phytoplankton bloom was observed less than 2 days after the main eruption
- Ocean fertilization through volcanic ash deposition likely fueled the bloom
- Strong temperature anomalies indicate localized volcanogenic upwelling near the caldera

Abstract

The largest volcanic eruption of this century, which was submarine, led to a dramatic phytoplankton bloom north of the island of Tongatapu, in the Kingdom of Tonga. In the absence of shipboard observations, we reconstructed the dynamics of this event by using a suite of satellite observations. Two independent bio-optical approaches confirmed that the phytoplankton bloom was a robust observation and not an optical artifact due to volcanogenic material. Furthermore, the timing, size, and position of the phytoplankton bloom suggest that plankton growth was primarily stimulated by nutrients released from volcanic ash rather than by nutrients upwelled through submarine volcanic activity. The appearance of a large region with high chlorophyll *a* concentrations less than 48 hours after the largest eruptive phase indicates a fast ecosystem response to nutrient fertilization. However, net phytoplankton growth probably initiated before the main eruption, when weaker volcanism had already fertilized the ocean.

1 Introduction

The submarine Hunga Tonga–Hunga Ha apai (HTHH) volcano erupted violently on January 15 2022 after several weeks of intermittent activity, first detected on December 20, 2021 (Zhao et al., 2022). A subaerial eruption phase began at 3:20 pm GMT on Jan 13 when the volcano emitted a plume of ash, steam, and gas with ashfall being reported on several nearby inhabited islands (Global Volcanism Program, 2022a). The main submarine eruption began around 4:00 am GMT on Jan 15 and was associated with the emission of a large plume of

ash, which reached an altitude of 58 km (NASA report, 2022). Ash deposition caused much damage on several Tongan islands (Witze, 2022) and the Tsunami wave train that followed the eruption caused further damage and five confirmed deaths. While the most dramatic consequences for humanity were experienced on land, various impacts also occurred in the ocean; here, we try to disentangle the ecological dynamics of the surface ocean caused by this eruption.

Volcanic activity can influence surface ocean ecosystems through different mechanisms, many of which result from the addition of growth-limiting nutrients. After an eruption, the deposition of volcanic ash can support the release of nutrient-containing materials in seawater (Duggen et al., 2007; Duggen et al., 2010; Frogner et al., 2001; Jones and Gislason, 2008), which has been previously invoked as the mechanism responsible for the formation of a large phytoplankton bloom in the North Pacific Ocean (Hamme et al., 2010; Langmann et al., 2010). In addition, nutrients can be delivered from depth, when warm and low-density water masses rise toward the sea surface. Upwelling can be caused by the emission of large volumes of hydrothermal fluids and by the exchange of heat between nutrient-rich seawater and a lava extrusion, following a submarine eruption (Baker et al., 1987; Baker et al., 2012; Butterfield et al., 1997; Vogt, 1989; Wilson et al., 2019). These mechanisms of ocean fertilization can provide large quantities of dissolved iron to the ocean ecosystem, which could favor the growth of specific organisms such as nitrogen fixing cyanobacteria, whose iron requirement is large (Karl et al., 2002).

Despite being Earth's dominant form of volcanism, submarine volcanic activity is understudied relative to eruptions on land due to challenges related to monitoring, observing, and sampling submarine geological features. However, some aspects of underwater volcanism are relatively established and we know that a large concentration of the most explosive underwater volcanoes lies near the Earth's subduction zones such as the one forming the primary Tongan islands (Rubin et al., 2012). Common indicators of shallow submarine volcanic activity are subaerial eruption columns, pumice rafts, and discolored seawater, all detectable through satellite observations. Seawater discoloration is caused by a combination of volcanic tephra, its weathering products, and suspended mineral precipitates including iron, aluminum, and silicon hydrous oxides (Urai and Machida, 2005).

HTHH is one of a half dozen volcanoes on Tongas Central Tofua arc that have erupted this century (e.g., Brandl et al., 2020 and references therein). The historical activity of HTHH is well documented in the scientific literature. Before the twenty first century, eruptions were reported in 1912, 1937, and 1988 (Bryan et al., 1972; Global Volcanism Program, 1988). More recently, two major eruptions were reported in March 2009 and January 2015 (Global Volcanism Program, 2009; Global Volcanism Program, 2015; Vaughan and Webley, 2010), which caused significant changes to the volcanic edifice both above and below sea level (Cronin et al., 2017; Garvin et al., 2018).

Submarine volcanic activity near Tonga has been linked with the presence of

discolored water and the formation of pumice rafts stretching for tens of km (Mantas et al., 2011; Vaughan and Webley, 2010). Early reports on the volcanic activity of HTHH in December 2021 also documented the presence of surface ocean pumice rafts (Global Volcanism Report, 2022b).

The region of the subtropical South Pacific Ocean near HTHH is characterized by low phytoplankton biomass, and low inorganic nitrogen concentration in the upper 80–100 m of the water column (Bonnet et al., 2018). Several weeks after the 2015 eruption of the HTHH volcano, Guieu et al. (2018) measured large concentrations of dissolved iron in the seawater near the Tongan islands, which they proposed to derive from emissions of hydrothermal fluids from nearby volcanoes. During the same expedition, Bonnet et al. (2018) measured large rates of nitrogen fixation by *Trichodesmium* between Tonga and New Caledonia, which were linked with the large iron concentration in the region. *Trichodesmium* was already observed to form a bloom along the northern coast of the island of Tongatapu, in 1963 (Bowman and Lancaster, 1965). This bloom appeared gray, an unusual color for the cyanobacterium, which led "some observers" (sic.) to hypothesize that the water contained suspended ash originated from an underwater eruption.

In our investigation, we looked at the dramatic stimulation of phytoplankton growth following the 2022 HTHH eruption. To infer the dynamics leading to this large phytoplankton bloom, we used a suite of satellite observations that helped us constrain the nature of the volcanic nutrient inputs and the scales of the ecological response.

2 Remote observations and models

2.1 Chlorophyll *a* concentration and fluorescence

We used two bio-optical measurements to assess changes in phytoplankton biomass before and after the HTHH eruption. The first bio-optical measurement is chlorophyll *a*, the primary pigment in photosynthesis, whose concentration in the first optical depth was obtained as the level 3, near real-time Globcolour data product distributed by the Copernicus Marine Service. These daily chlorophyll *a* maps have a horizontal resolution of 4 km and merge measurements from different sensors including SeaWiFS, MODIS, MERIS, VIIRS, and OLCI. Chlorophyll *a* estimates are based on the CI-Hu algorithm in oligotrophic waters and the OC5 algorithm in mesotrophic and coastal waters (Gohin et al., 2002; Hu et al., 2012). These empirical remote-sensing algorithms are loosely based on differences in seawater reflectance between blue light, which is absorbed by chlorophyll *a*, and green light, which is not absorbed by chlorophyll *a*. Missing observations in the daily Globcolour maps were filled using a least square approach to calculate the bloom area and plot its contour.

A second bio-optical proxy for phytoplankton biomass is based on measurements of the red fluorescence emitted by chlorophyll *a*, when exposed to sunlight (Letelier and Abbott, 1996). The algorithm uses differences in water leaving radiance measured from the MODIS sensors in two red wavebands and calculates normal-

ized fluorescence line height (nFLH), which we later corrected to account for differences in non-photochemical quenching (Behrenfeld et al., 2009). Henceforth, we simply use the term nFLH to indicate measurements corrected for differences in the degree of non-photochemical quenching. We compared nFLH and chlorophyll *a* retrievals using Level 2 images collected by the MODIS Aqua satellite before and after the HTHH eruptive activity.

2.2 Sea surface temperature

Remote sensing of sea surface temperature (SST) is based on measurements from numerous satellites, and it relies on algorithms using wavelengths in the infrared or microwave spectral bands. To identify SST anomalies, we analyzed the measurements collected by several satellites, which all indicated similar SST fields. Herein, we describe the SST anomalies by reporting measurements retrieved using the infrared bands of the VIIRS sensor onboard the NOAA20 satellite.

While there are data products merging SST observations made by different remote platforms, which improve on the spatial coverage obtained by any single platform, we opted for not using this approach because the temporal and spatial interpolation schemes of the merged products seemed to preclude the precise identification of the time of appearance and position of the SST anomalies.

2.3 Surface currents

The direction and magnitude of ocean currents in the top 30 m of the water column were obtained from the Ocean Surface Current Analyses Real-time (OSCAR). This daily data product has a spatial resolution of 0.25° in latitude and longitude (~27 km), and the calculation of the currents takes into account a geostrophic term, a wind-driven term, and a thermal wind adjustment.

2.4 True color satellite images

The aerial plume emitted by the HTHH volcano was characterized using true color images obtained with the GeoColor technique applied to measurements from the Geostationary Operational Environmental Satellite (GOES) West (Miller et al., 2020). Considering the height of the plume with respect to sea level, we suspect that the coordinates assigned to the pixels of the plume cloud were impacted by a projection error. Since the GOES West satellite is northeast of HTHH, the plume was probably projected southwest of its true position perpendicular to the earth's surface.

3 Results

Chlorophyll *a* concentrations near HTHH increased tenfold from values near 0.1 mg m^{-3} on Jan 11, before the eruption, to values near 1 mg m^{-3} on Jan 16, less than two days after the main eruptive event (Figure 1). A large region (~200 km in the zonal direction) of enhanced chlorophyll *a* with respect to the monthly average value of 0.1 mg m^{-3} was still present on Jan 21 and for several days afterward (Figure 1).

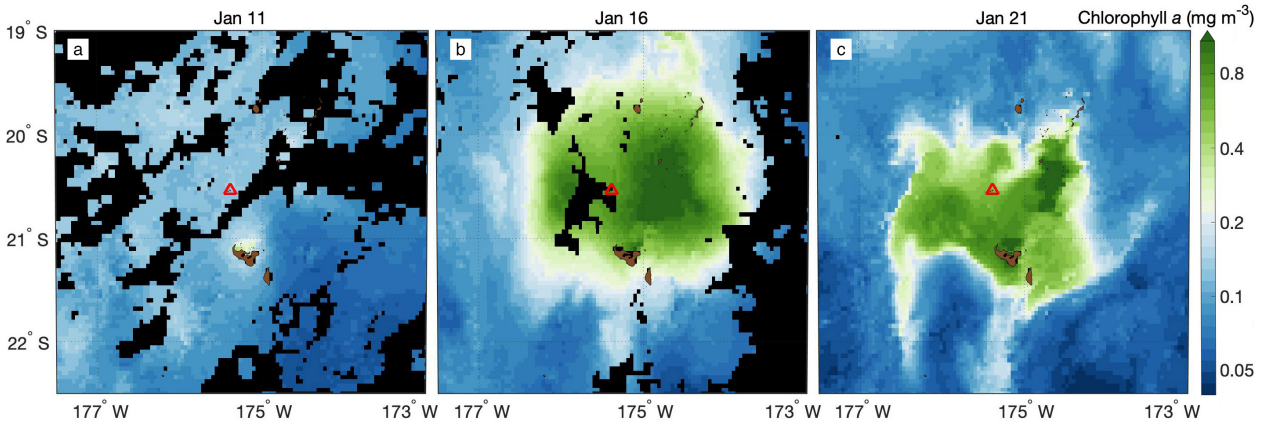

Figure 1: Concentrations of chlorophyll a spanning a period of 10 days in the region near HTHH, whose position is depicted as a red triangle. a) January 11, before the main HTHH eruption; b) January 16, with the first available observations after the main eruption; c) January 21, 6 days after the eruption. The largest landmass (brown in the figure) to the south of HTHH is the island of Tongatapu. Black areas depict missing observations.

The chlorophyll *a* anomaly observed starting on Jan 16 is unprecedented in the time-series measured during the satellite era, starting in 1997 (Figure 2a). Review of archive data from the region of interest indicated that prior to the 2022 HTHH eruption, satellites never recorded an average chlorophyll *a* concentration anywhere close to 1 mg m^{-3}. However, two other events with anomalously high chlorophyll *a* concentrations and smaller areal extents were recorded in Jan 2015 and Jan 2017 (Figure 2a). Both events were linked with documented eruptive activity: The 2015 event was associated with an eruption of the HTHH volcano and the 2017 event coincided with the activity of an unnamed submarine volcano southwest of HTHH. Chlorophyll *a* near HTHH progressively declined after January 17 and reached typical climatological values on January 27 (Figure 2b). A similar decrease was observed in the area of enhanced chlorophyll *a*, here defined as having concentrations > 0.2 mg m^{-3}, which was 60,926 km^2 on January 16 and only 12,053 km^2 on January 28 (Figure

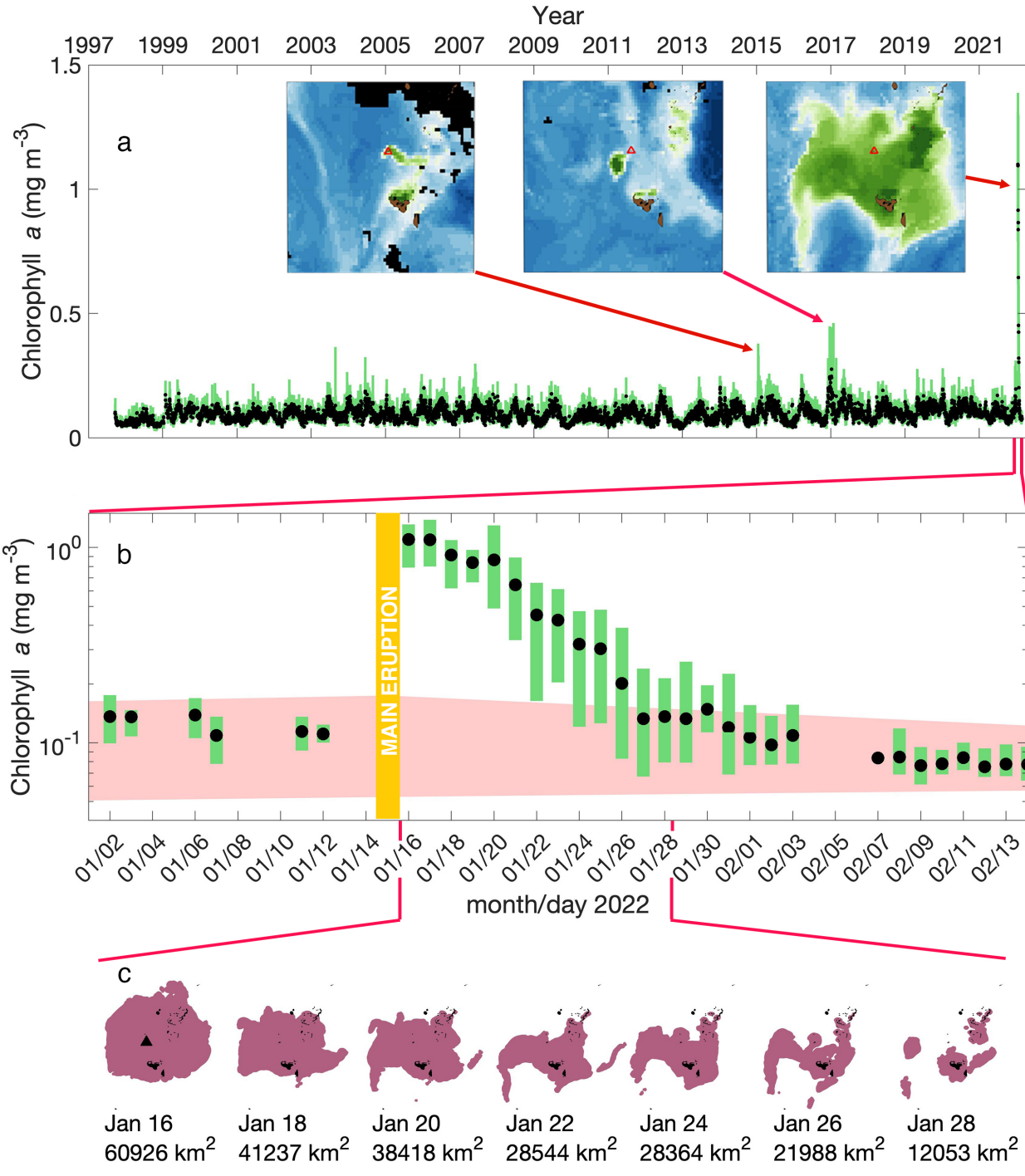
Year
1997 1999 2001 2003 2005 2007 2009 2011 2013 2015 2017 2019 2021
a
Chlorophyll a (mg m-3)
1.5
1
0.5
0
b
Chlorophyll a (mg m-3)
10^0
10^-1
MAIN ERUPTION
01/02 01/04 01/06 01/08 01/10 01/12 01/14 01/16 01/18 01/20 01/22 01/24 01/26 01/28 01/30 02/01 02/03 02/05 02/07 02/09 02/11 02/13
month/day 2022
c
Jan 16
60926 km2
Jan 18
41237 km2
Jan 20
38418 km2
Jan 22
28544 km2
Jan 24
28364 km2
Jan 26
21988 km2
Jan 28
12053 km2

2c).

Figure 2: Chlorophyll a distribution in the region of the HTHH volcano. a) Time-series of chlorophyll a during the satellite era in the coordinate box between 20.3–20.9°S and 174.8–175.9°W. b) Same as a), but for the first part of year 2022 showing the increase in chlorophyll a and its decline following the HTHH eruption of January 15. c) Contour of the area with chlorophyll a >0.2 mg m^{-3} after the January 15. The three panels in a) depict chlorophyll a maps associated with three documented volcanic events. Black symbols and green bars in a) and b) depict average and 5-95% of the concentration, respectively. The pink region in b) depict 5-95% of the concentrations from the monthly climatology in the coordinate box.

To constrain possible artifacts in the estimates of chlorophyll *a* concentrations due to suspended and dissolved volcanogenic material, we compared satellite maps of absorption-based chlorophyll *a* and fluorescence-based nFLH. Both approaches estimated low values in the HTHH region on December 16, 2021, before the beginning of the volcanic activity, but a large region with high chlorophyll *a* concentration and sun-induced fluorescence on Jan 17, 2022 (Fig. 3).

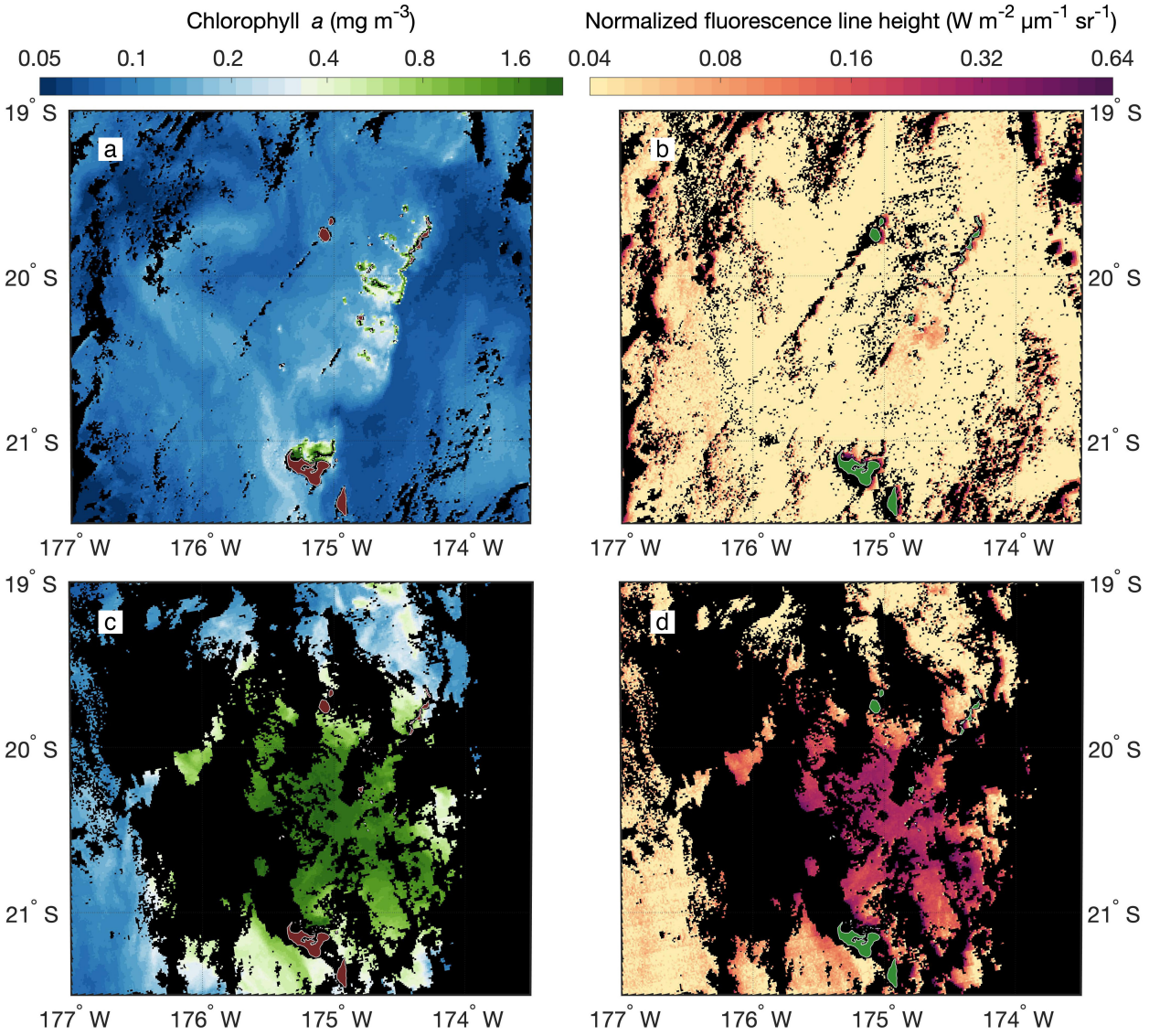

Figure 3:Estimates of chlorophyll a (a,c) and nFLH (b,d) from the MODIS Aqua satellite. a,b) Satellite image from December 16, 2021, before the beginning of the HTHH volcanic activity; c,d) Satellite image from Jan 17, 2022, two days after the main eruption of the HTHH volcano. Values of nFLH have been corrected for changes in non-photochemical quenching. Black areas depict missing observations.

The spatial coverage of satellite SST near HTHH was low in the days immediately following the Jan 15, 2022 eruption, likely due to the presence in the atmosphere of volcanic tephra, sulfate aerosol, and gas clouds associated with

the volcanic activity. Nonetheless, SST from the NOAA20 satellite on Jan 17 shows temperatures above 30°C near HTHH in what could be interpreted as the edge of a region of high SST anomaly extending to the southwest, where satellite observations are missing (Figure 4). During the following days, the high-SST water mass was observed progressively more to the southwest of HTHH, consistent with the direction and magnitude of the ocean currents predicted by the OSCAR model (Figure 4).

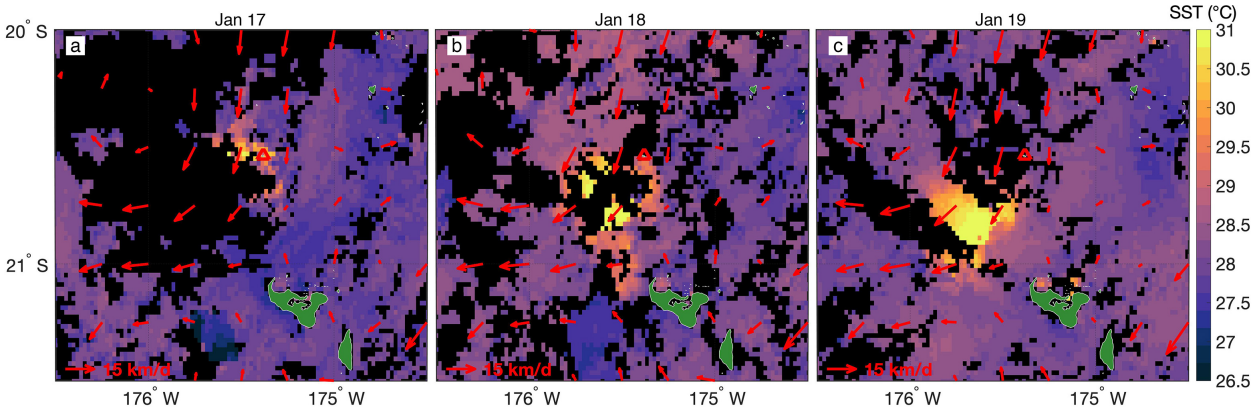

Figure 4: SST and surface currents after the eruption of the HTHH volcano on a) January 17, b) January 18, and c) January 19. The red triangle depicts the position of HTHH. Red arrows depict ocean currents in the upper 30 m. Black areas depict missing observations.

We qualitatively assessed the likelihood and magnitude of ash deposition by visual analysis of the volcanic plume generated by HTHH. On January 13, before the main eruptive phase of HTHH, a weaker eruption had already generated a large atmospheric plume above the region of the ocean that would later be hosting the phytoplankton bloom (Figure 5a). About 1.5 days later, the largest blast of January 15 reached further away from HTHH (Figure 5b). True color images also revealed the presence of flotsam, after the main eruption (Supplementary Information).

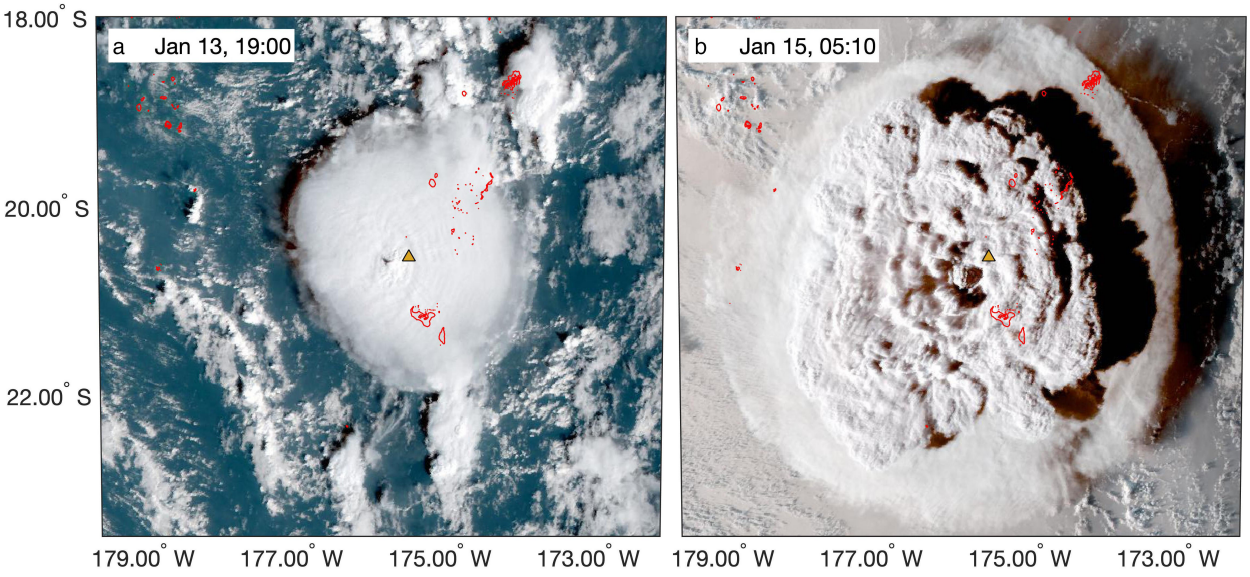

Figure 5: True color images of the HTHH region from the geostationary satellite GOES-West. a) Aerial emission linked with the volcanic activity on January 13; b) Ash plume emitted during the main eruption on January 15. Red lines depict the coastline and the yellow triangle depicts the position of the HTHH volcano.

4 Discussion and Conclusions

Satellite observations revealed many impacts of the HTHH eruption on the nearby ocean, but the most striking signal was a large phytoplankton bloom first detected on January 16. Previous studies in the region of the Canary Islands reported an overestimation in satellite estimates of chlorophyll *a* concentration due to discolored waters emitted through submarine volcanic activity (Coca et al., 2014; Gómez Letona, 2017). Hence, we verified that the Tongan phytoplankton bloom was not an artifact by confirming its presence using both absorption-based and fluorescence-based bio-optical approaches.

In the oligotrophic region of the ocean surrounding HTHH, a surface phytoplankton bloom can only develop if growth-limiting nutrients are supplied to the upper ocean. The HTHH eruption could have supplied these nutrients both from above, through atmospheric ash deposition, and from below, through the upwelling of seawater containing a volcanogenic component (hydrothermal fluids, water that came into contact with hot magmatic products, or condensed volcanic vapors emitted into seawater). Both mechanisms have been proposed previously (Baker et al., 1987; Butterfield et al., 1997; Frogner et al., 2001). However, the implied upward and downward nutrient fluxes have different spatial and temporal scales, whereby the atmospheric route is faster and can reach greater distances over a specific time frame.

The upwelling of warm water near the HTHH caldera is evident in the warm

water anomaly observed in satellite images, which was progressively advected southwest of HTHH. The upwelled water must have mixed with the cooler ambient seawater already present at the sea surface so we can safely assume that the region impacted by nutrient upwelling was larger than the region of the SST anomaly. However, it would be hard to attribute the large chlorophyll *a* anomalies northeast of HTHH solely to nutrient upwelling, considering that the water would have had to be advected against the direction of the currents predicted in the study region.

For the reason above, we believe that phytoplankton growth was mostly stimulated by the release of nutrients present on the surface or inside juvenile volcanic ash and tephra products. Depositional patterns from the 2014-2015 HTHH eruption (Cronin et al., 2017) and application of volcanic ash deposition models (Bonadonna et al., 1998; Hurst and Davis, 2017) indicate a likely ash deposition thickness of 100–1000 cm in the region of the chlorophyll *a* anomaly. Could this amount of ash have leached enough nutrients to sustain a phytoplankton biomass equivalent to 1 mg m^{-3} of chlorophyll *a*? A calculation of the nutrient flux through this process can be obtained by using the rate of nutrient release in the top 50 m from the deposition of subduction zone volcanic ash reported by Duggen et al. (2007). Following these authors' calculation and assuming a conservative ash deposition of 100 cm, we obtain fluxes of 1.0–3.2 mol m^{-3} of inorganic nitrogen (N), 0.4–4 mmol m^{-3} of phosphorus (P), and 0.4–2.4 mmol m^{-3} of iron (Fe). By assuming a Redfield stoichiometry for the synthesis of phytoplankton biomass and 10 moles of P per mole of Fe, the release rates reported by Duggen et al. (2007) indicate that P would be depleted before N and Fe. Even so, with a ratio of 100 g of carbon per g of chlorophyll *a*, the P supplied through ash deposition could account for 5–50 mg m^{-3} of chlorophyll *a*, well in excess of the maximum concentration observed in the study region.

The time scale of the chlorophyll *a* increase is also informative on the dynamics leading to the phytoplankton bloom. In the coordinate box selected for the time-series of Figure 2, we measured an average chlorophyll *a* concentration of 0.11 mg m^{-3} on January 12, before the eruptions, and 1.10 mg m^{-3} on January 16. If we assume that phytoplankton growth started after the main eruption (4 am on January 15) the implied exponential rate of chlorophyll *a* increase would be 2.2 d^{-1} (using a growth period of 1.06 days based on the average hours of illumination from the eruption to January 16 GMT). While fast-growing phytoplankton species can achieve this high intrinsic growth rate in warm water (Bissinger et al., 2008), net growth of the dominant phytoplankton species starting from a small seed population is unlikely to result in such a fast chlorophyll *a* increase. As a reference, in conditions of nutrient sufficiency, the relatively fast rates of chlorophyll *a* accumulation were always <0.6 d^{-1} during artificial iron amendments, and 1.0 d^{-1} during incubations with added nutrients (Figure 1 of Behrenfeld and Boss, 2014; McAndrew et al., 2007; Mahaffey et al., 2012). For this reason, it is likely that net phytoplankton growth did not begin on January 15, but it had already been stimulated by the less intense HTHH eruption of January 13. Even though we consider this the most realistic hypothesis, we

cannot directly verify it with available chlorophyll *a* observations, which are regionally too sparse on Jan 14 and Jan 15, likely due to the low visibility after the eruptions.

The HTHH eruption of Jan 15 2022 was a very large geophysical event leading to a rare physical and chemical perturbation of an oligotrophic pelagic ecosystem. In the absence of more comprehensive shipboard observations to characterize the response of the ecosystem, we must rely on remote measurements to identify the most likely dynamics that led to the tenfold chlorophyll *a* increase measured in an area spanning tens of thousands of square kilometers. Our observations are consistent with an input of nutrients supplied through ash deposition, which stimulated primary production and, most likely, particle export on short temporal scales. However, based on the published composition of subduction zone volcanic ash, this nutrient flux could eventually lead to phosphorus limitation in the region.

Acknowledgments

We thank the personnel from NASA and the Copernicus Marine Service who curated and oversaw the distribution of the satellite observations used in this study. This work was supported by a grant from the Simons Foundation (#329108-721252 to DMK).

Open Research

Chlorophyll *a* data are available from the Copernicus Marine Service (https://marine.copernicus.eu/, doi:10.48670/moi-00096 and doi:10.48670/moi-00098). MODIS Aqua images are available from NASA's OceanColor (https://oceancolor.gsfc.nasa.gov/, doi:10.5067/AQUA/MODIS/L2/OC/2018). SST data are distributed by NASA's Physical Oceanography Distributed Active Archive Center (https://podaac.jpl.nasa.gov/, doi:10.5067/GHV20-3UO61). OSCAR is generated by Earth & Space Research and distributed by NASA's Earthdata (https://earthdata.nasa.gov/, doi:10.5067/OSCAR-25N20). True color geostationary images are available from NASA Worldview (https://worldview.earthdata.nasa.gov/).

References

Baker, E. T., Massoth, G. J., & Feely, R. A. (1987). Cataclysmic hydrothermal venting on the Juan de Fuca Ridge. *Nature*, *329*(6135), 149-151.

Baker, E. T., Chadwick Jr, W. W., Cowen, J. P., Dziak, R. P., Rubin, K. H., & Fornari, D. J. (2012). Hydrothermal discharge during submarine eruptions: The importance of detection, response, and new technology. *Oceanography*, *25*(1), 128-141.

Behrenfeld, M. J., & Boss, E. S. (2014). Resurrecting the ecological underpinnings of ocean plankton blooms. *Annual Review of Marine Science*, 6, 167-194.

Behrenfeld, M. J., Westberry, T. K., Boss, E. S., O'Malley, R. T., Siegel, D. A., Wiggert, J. D., ... & Mahowald, N. (2009). Satellite-detected fluorescence reveals global physiology of ocean phytoplankton. *Biogeosciences*, 6(5), 779-794.

Bissinger, J. E., Montagnes, D. J., harples, J., & Atkinson, D. (2008). Predicting marine phytoplankton maximum growth rates from temperature: Improving on the Eppley curve using quantile regression. *Limnology and Oceanography*, 53(2), 487-493. https://doi.org/10.4319/lo.2008.53.2.0487

Bonadonna, C., Ernst, G. G. J., & Sparks, R. S. J. (1998). Thickness variations and volume estimates of tephra fall deposits: the importance of particle Reynolds number. *Journal of Volcanology and Geothermal Research*, 81(3-4), 173-187.

Bonnet, S., Caffin, M., Berthelot, H., Grosso, O., Benavides, M., Helias-Nunige, S., ... & Foster, R. A. (2018). In-depth characterization of diazotroph activity across the western tropical South Pacific hotspot of N_2 fixation (OUTPACE cruise). *Biogeosciences*, *15*(13), 4215-4232.

Bowman, T. E., & Lancaster, L. J. (1965). A bloom of the planktonic blue–green alga, *Trichodesmium Erythraeum*, in the Tonga islands. *Limnology and Oceanography*, 10(2), 291-293.

Brandl, P. A., Schmid, F., Augustin, N., Grevemeyer, I., Arculus, R. J., Devey, C. W., ... & Hannington, M. D. (2020). The 6–8 Aug 2019 eruption of 'Volcano F'in the Tofua Arc, Tonga. *Journal of Volcanology and Geothermal Research*, 390, 106695.

Bryan, W. B., Stice, G. D., & Ewart, A. (1972). Geology, petrography, and geochemistry of the volcanic islands of Tonga. *Journal of Geophysical Research*, *77*(8), 1566-1585.

Butterfield, D. A., Jonasson, I. R., Massoth, G. J., Feely, R. A., Roe, K. K., Embley, R. E., ... & Delaney, J. R. (1997). Seafloor eruptions and evolution of hydrothermal fluid chemistry. *Philosophical Transactions of the Royal Society of London. Series A: Mathematical, Physical and Engineering Sciences*, *355*(1723), 369-386.

Coca, J., Ohde, T., Redondo, A., García-Weil, L., Santana-Casiano, M., González-Dávila, M., ... & Ramos, A. G. (2014). Remote sensing of the El Hierro submarine volcanic eruption plume. *International Journal of Remote Sensing*, *35*(17), 6573-6598.

Cronin, S. J., Brenna, M., Smith, I. E. M., Barker, S. J., Tost, M., Ford, M., Tonga'onevai, S., Kula, T., & Vaiomounga, R. (2017). New volcanic island unveils explosive past, *Eos*, 98, https://doi.org/10.1029/2017EO076589

Duggen, S., Croot, P., Schacht, U., & Hoffmann, L. (2007). Subduction zone volcanic ash can fertilize the surface ocean and stimulate phytoplankton growth: Evidence from biogeochemical experiments and satellite data. *Geophysical Research Letters*, *34*(1).

Duggen, S., Olgun, N., Croot, P., Hoffmann, L., Dietze, H., Delmelle, P., & Teschner, C. (2010). The role of airborne volcanic ash for the surface ocean biogeochemical iron-cycle: a review. *Biogeosciences*, *7*(3), 827-844.

Flynn, K. J., & Raven, J. A. (2017). What is the limit for photoautotrophic plankton growth rates?. *Journal of Plankton Research*, 39(1), 13-22.

Frogner, P., Gíslason, S. R., & Oskarsson, N. (2001). Fertilizing potential of volcanic ash in ocean surface water. *Geology*, 29(6), 487-490.

Garvin, J.B., D.A. Slayback, V. Ferrini, J. Frawley, C. Giguere, G.R. Asrar, & K. Andersen (2018). Monitoring and modeling the rapid evolution of earth's newest volcanic island: Hunga Tonga Hunga Ha'apai (Tonga) using high spatial resolution satellite observations. *Geophysical Research Letters*, 45. https://doi.org/10.1002/2017GL076621

Global Volcanism Program (1988). Report on Hunga Tonga-Hunga Ha'apai (Tonga) (McClelland, L., ed.). *Scientific Event Alert Network Bulletin*, 13:5. Smithsonian Institution. https://doi.org/10.5479/si.GVP.SEAN198805-243040

Global Volcanism Program (2009). Report on Hunga Tonga-Hunga Ha'apai (Tonga) (Venzke, E. A., and Wunderman, R., eds.). *Bulletin of the Global Volcanism Network*, 34:3. Smithsonian Institution. https://doi.org/10.5479/si.GVP.BGVN200903-243040

Global Volcanism Program (2015). Report on Hunga Tonga-Hunga Ha'apai (Tonga), (Wunderman, R., ed.). *Bulletin of the Global Volcanism Network*, 40:1. Smithsonian Institution. https://doi.org/10.5479/si.GVP.BGVN201501-243040

Global Volcanism Program (2022a). Report on Hunga Tonga-Hunga Ha'apai (Tonga). (Sennert, S. K., ed.), *Weekly Volcanic Activity Report*, 12 January-18 January 2022. Smithsonian Institution and US Geological Survey.

Global Volcanism Program (2022b). Report on Hunga Tonga-Hunga Ha'apai (Tonga) (Crafford, A. E., and Venzke, E., eds.). *Bulletin of the Global Volcanism Network*, 47:2. Smithsonian Institution.

Gohin, F., Druon, J. N. & Lampert, L. (2002). A five channel chlorophyll concentration algorithm applied to SeaWiFS data processed by SeaDAS in coastal waters. *International Journal of Remote Sensing*, 23(8), 1639-1661, https://doi.org/10.1080/01431160110071879.

Gómez Letona, M. (2017). Did the submarine volcanic eruption of El Hierro (Canary Islands) lead to a biological fertilization of the planktonic community?: evidences from "in situ" and remote sensing data in the phytoplanktonic community (Master's thesis).

Guieu, C., Bonnet, S., Petrenko, A., Menkes, C., Chavagnac, V., Desboeufs, K., ... & Moutin, T. (2018). Iron from a submarine source impacts the productive layer of the Western Tropical South Pacific (WTSP). *Scientific Reports*, *8*(1), 1-9.

Hamme, R. C., Webley, P. W., Crawford, W. R., Whitney, F. A., DeGrandpre, M. D., Emerson, S. R., ... & Lockwood, D. (2010). Volcanic ash fuels anomalous plankton bloom in subarctic northeast Pacific. *Geophysical Research Letters*, *37*(19).

Hu, C., Lee, Z. & Franz, B. (2012). Chlorophyll *a* algorithms for oligotrophic oceans: A novel approach based on three-band reflectance difference. *Journal of Geophysical Research: Oceans*, 117(C1). https://doi.org/10.1029/2011jc007395.

Hurst, T. & Davis, C. (2017). Forecasting volcanic ash deposition using HYSPLIT. *Journal of Applied Volcanology*, 6, 5. https://doi.org/10.1186/s13617-017-0056-7.

Jones, M. T., and Gislason, S. R. (2008). Rapid releases of metal salts and nutrients following the deposition of volcanic ash into aqueous environments. *Geochimica et Cosmochimica Acta*, 72(15), 3661-3680.

Karl, D., Michaels, A., Bergman, B., Capone, D., Carpenter, E., Letelier, R., ... & Stal, L. (2002). Dinitrogen fixation in the world's oceans. *Biogeochemistry*, 57(1), 47-98.

Langmann, B., Zakšek, K., Hort, M., & Duggen, S. (2010). Volcanic ash as fertiliser for the surface ocean. *Atmospheric Chemistry and Physics*, *10*(8), 3891-3899.

Letelier, R. M., & Abbott, M. R. (1996). An analysis of chlorophyll fluorescence algorithms for the Moderate Resolution Imaging Spectrometer (MODIS). *Remote Sensing of Environment*, 58(2), 215-223.

Mahaffey, C., Björkman, K. M., & Karl, D. M. (2012). Phytoplankton response to deep seawater nutrient addition in the North Pacific Subtropical Gyre. *Marine Ecology Progress Series*, 460, 13-34. https://doi.org/10.3354/meps09699

Mantas, V. M., Pereira, A. J. S. C., & Morais, P. V. (2011). Plumes of discolored water of volcanic origin and possible implications for algal communities. The case of the Home Reef eruption of 2006 (Tonga, Southwest Pacific Ocean). *Remote Sensing of Environment*, *115*(6), 1341-1352.

McAndrew, P. M., Björkman, K. M., Church, M. J., Morris, P. J., Jachowski, N., Williams, P. J. L. B., & Karl, D. M. (2007). Metabolic response of oligotrophic plankton communities to deep water nutrient enrichment. *Marine Ecology Progress Series*, 332, 63-75.

https://doi.org/10.3354/meps332063

Miller, S. D., Lindsey, D. T., Seaman, C. J., & Solbrig, J. E. (2020). GeoColor: A blending technique for satellite imagery. *Journal of Atmospheric and Oceanic Technology*, 37(3), 429-448. https://doi.org/10.1175/JTECH-D-19-0134.1

NASA report (2022). https://earthobservatory.nasa.gov/images/149474/tonga-volcano-plume-reached-the-mesosphere

Planet Team (2017). *Planet Application Program Interface: In Space for Life on Earth*. San Francisco, CA. https://api.planet.com.

Rubin, K. H., Soule, S. A., Chadwick Jr, W. W., Fornari, D. J., Clague, D. A., Embley, R. W., ... & Dziak, R. P. (2012). Volcanic eruptions in the deep sea. *Oceanography*, *25*(1), 142-157.

Urai, M., & Machida, S. (2005). Discolored seawater detection using ASTER reflectance products: A case study of Satsuma-Iwojima, Japan. *Remote Sensing of Environment*, *99*(1-2), 95-104.

Vaughan, R. G., & Webley, P. W. (2010). Satellite observations of a Surtseyan eruption: Hunga Ha'apai, Tonga. *Journal of Volcanology and Geothermal Research*, *198*(1-2), 177-186.

Vogt, P. R. (1989). Volcanogenic upwelling of anoxic, nutrient-rich water: A possible factor in carbonate-bank/reef demise and benthic faunal extinctions?. *Geological Society of America Bulletin*, *101*(10), 1225-1245.

Wilson, S. T., Hawco, N. J., Armbrust, E. V., Barone, B., Björkman, K. M., Boysen, A. K., ... & Karl, D. M. (2019). Kīlauea lava fuels phytoplankton bloom in the North Pacific Ocean. *Science*, 365(6457), 1040-1044.

Witze, A. (2022). Why the Tongan eruption will go down in the history of volcanology. *Nature*, *602*(7897), 376-378.

Zhao, W., Sun, C., and Guo, Z. (2022). Reawakening of Tonga volcano. *The Innovation*. 3(2).